Science of the Total Environment 898 (2023) 165558

Contents lists available at ScienceDirect

Science of the Total Environment

journal homepage: www.elsevier.com/locate/scitotenv

Modelling biogeochemical reactions triggered by graphene's addition in a fertilized calcareous sandy soil

Luigi Alessandrino [a], Nicolò Colombani [b,*], Micòl Mastrocicco [a]

[a] DiSTABiF - Department of Environmental, Biological and Pharmaceutical Sciences and Technologies, Campania University "Luigi Vanvitelli", Via Vivaldi 43, 81100 Caserta, Italy
[b] SIMAU - Department of Materials, Environmental Sciences and Urban Planning, Marche Polytechnic University, Via Brecce Bianche 12, 60131 Ancona, Italy

ARTICLE INFO

Editor: Daniel S Alessi

Keywords:
Numerical model
Reactive transport
Denitrification
Column experiments
Nutrients leaching

ABSTRACT

Graphene production has dramatically increased in the last years and new ways to recycle this engineered material need to be investigated. To this purpose, a reactive model network was developed using PHREEQC-3 code to quantify the relevant biogeochemical reactions induced by graphene scraps' incorporation in a calcareous sandy soil. The numerical model was calibrated versus a complete dataset of column experiments in water saturated conditions using two different fertilizers, a synthetic NPK fertilizer and fertigation water produced in a wastewater treatment plant. Column experiments consisted of 50 cm columns filled with a mixture of graphene scraps (0.015 % dry weight) and soil in the first 10 cm, while the remaining 40 cm had only soil. The model performance was tested using classical statistical indices (R^2, Modelling Efficiency, and Index of Agreement), resulting to be satisfactory. Besides, a simple sensitivity analysis via the perturbation of relevant parameters showed a low degree of uncertainty. The main outcome of this study was the quantification of the increased denitrification rate triggered by graphene incorporation into the soil. Moreover, graphene incorporation substantially increased soil CEC and DOC sorption capacity, demonstrating a good adsorption capacity for ammonium and organic compounds, thus decreasing nutrients leaching that represents a major concern related to agricultural practice. Indeed, Graphene incorporation increased by 40 % the CEC in the first 10 cm of the CSG_NPK column ($2.50e^{-02}$ mol/L) respect to the CS_NPK column ($1.75e^{-02}$ mol/L) and increased it by 150 % in the first 10 cm of the CSG_FW column ($2.50e^{-02}$ mol/L) in comparison with the CS_FW column $1.00e^{-02}$ (mol/L). pH fluctuations were most likely due to the precipitation of $Ca_5(PO_4)_3OH$, indeed the consumption of H^+ ions could have triggered the pH lowering during the experiment. These results could be relevant for future graphene applications as a soil improver or as suitable material to enhance soil bioremediation in order to include graphene in a circular economy loop.

1. Introduction

Sandy soils are renowned for their low water holding capacity, low cation exchange capacity (CEC) and low fertility since they are typically deficient in organic matter and nutrients (Dafny and Šimůnek, 2016; Gruba and Mulder, 2015; Novak and Watts, 2004; Reichert et al., 2016). Sandy soils are often over-fertilized to offset these inherent disadvantages (Ellmer et al., 2000), so that nutrient leaching is higher in sandy soils than in soils with fine texture (Di and Cameron, 2002). Organic and inorganic soil improvers have been thoroughly tested to improve the physical and chemical properties of sandy soils and to reduce nutrients' leaching (Chan et al., 2007; Hardie et al., 2014; Plošek et al., 2017; White et al., 2014). Modern research is concentrating on the prospect of employing engineered nanomaterials to improve the quality of agricultural soils, despite the existence of numerous conventional soil improvers that are widely utilized (Bandala and Berli, 2018). Graphene is one of these nanomaterials and because of its unique properties, including strong resistance, outstanding electrical and thermal conductance, tremendous flexibility, and exceptional waterproofness, it is regarded to be very promising in many domains of application (Novoselov, 2011). The unprecedented growth in the number of developing graphene applications, as well as the number of patents submitted, may indicate the potential for graphene commercialization to accelerate further (Zurutuza and Marinelli, 2014). The direct functional

* Corresponding author.
E-mail address: n.colombani@univpm.it (N. Colombani).

https://doi.org/10.1016/j.scitotenv.2023.165558
Received 19 April 2023; Received in revised form 21 June 2023; Accepted 13 July 2023
Available online 15 July 2023

integration of graphene and other distinguishing building blocks, which can be substrates or materials introduced by transfer or epitaxial growth, is expected to spark new and unexpected graphene applications in industry (Lin et al., 2019). Despite graphene commercialization has been far from straightforward (Paton et al., 2014), the global graphene market is predicted to exceed US$800 million in the next years (Reiss et al., 2019). In addition, the new low-cost production techniques have caused its production to boost and in the coming years an increase in graphene-based waste and scraps is expected (Ruan et al., 2011; Tabish et al., 2018). Graphene has recently been tested on sandy soils in both batch and column experiments demonstrating its ability to decrease the leaching of nutrients and heavy metals (Alessandrino et al., 2022a, 2023), and to preserve the hydrodynamic characteristics of a soil (Alessandrino et al., 2022b). Despite the increasing number of papers focusing on graphene fate and transport in the subsurface (Sun et al., 2022), there is still a lack of studies using reactive transport models to quantify biogeochemical reactions induced in soils amended with graphene. One of the most complete and renown multicomponent reactive transport models is PHREEQC-3 (Parkhurst and Appelo, 2013), which is capable to simulate simple and complex biogeochemical reactions coupled with one dimensional advective-dispersive transport (Şengör and Ünlü, 2023; Sprocati et al., 2019; Steefel et al., 2015). PHREEQC-3 enables users to write BASIC scripts to describe rate equations for a wide range of kinetic biogeochemical reactions (Zhang et al., 2019). In this study, PHREEQC-3 was employed to assess the nutrients' leaching behaviour in different column experiments sourced from Alessandrino et al. (2023): (i) calcareous sandy soil under a NPK fertilization regime (CS_NPK), (ii) calcareous sandy soil amended with graphene under a NPK fertilization regime (CSG_NPK), (iii) calcareous sandy soil under a fertilization regime with fertigation water (FW) produced by a wastewater treatment plant (CS_FW), and (iv) calcareous sandy soil amended with graphene under a fertilization regime with fertigation water (CSG_FW). The reactive models were calibrated versus the observed solutes concentrations, and the rates of the major reactive processes were obtained and discussed along with literature values.

2. Materials and methods

2.1. Column experiments

The experimental data used to develop the reactive transport model were obtained from Alessandrino et al. (2023), where the experimental methodology and analytical methods are described in full detail. The experimental set-up is resumed in Fig. 1 and is briefly reported here. The column's filling was performed via 1–2 cm additions and each addition was packed with a Teflon piston before the next one was placed on top, to mimic the layering typical of alluvial environments. The topsoil (10 cm) was mixed with graphene to simulate the field practice, while the remaining 40 cm were filled just with soil (Fig. 1). The control columns were filled only with soil (50 cm). Columns were flushed via a peristaltic pump for at least 100 pore volumes to eliminate unwanted contaminants before each experiment. Column dimensions (5 cm of internal diameter and 50 cm of height) were set according to "ISO 21268-3:2019" standard in order to ensure a reasonable contact time between fluid and solid. For the saturated leaching experiment, the packed columns were completely saturated with distilled water. At the top and bottom of the columns, high density polyethylene (HDPE) chambers were installed to uniform the flux and to prevent washing of finer grains. The chambers contained an 80 HDPE pierced disc and a 50 μm NITEX mesh in contact with the soil. The flow direction was upward to avoid the formation of trapped gas bubbles in order to guarantee the reaching of the complete degree of saturation. The porewater flow rate was set at 4.2 mL/min via a peristaltic pump connected to the bottom of the column, ensuring a Darcian velocity (specific discharge) of approximately 30 cm/d. The leaching experiments followed this irrigation/fertilization scheme: first 100 mL of synthetic rainwater proxy (SRWP), then 300 mL of fertilizer (NPK or FW), and finally 600 mL of SRWP. A double port switch injector created a pulse input of fertilizer (NPK or FW). As soon as the injection of the fertilizer was completed, inflow was switched back to the SRWP while maintaining steady-state saturated flow conditions.

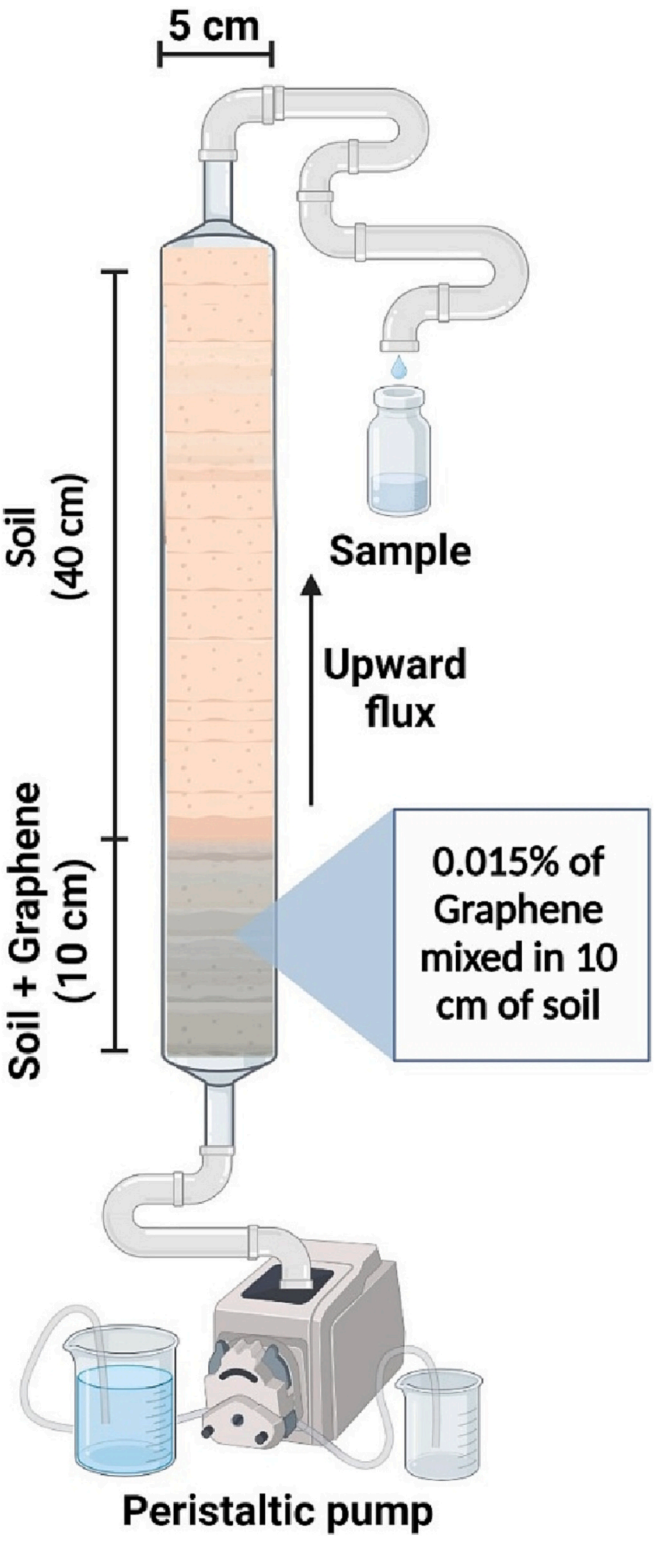

Fig. 1. Experimental column set up. The column was filled with a mixture of soil and graphene for the first 10 cm (from the bottom) and with soil only for the remaining 40 cm.

2.2. Reactive model framework and assumptions

Each column was discretized into nodal blocks termed as cells with similar pore volumes (Bethke and Brady, 2000) and with a fixed length of 1 cm, for a total of 50 cells. The main features of the flushing solution passing through the column (namely SRWP, NPK, and FW) are reported in Table 1. Generally, the leaching processes are complex so the main mechanisms considered in these simulations were the following: i) solutes transport; ii) cation exchange; iii) mineral dissolution/precipitation; and iv) kinetic reactions. Two models for each column experiment were performed, a non-reactive one considering only solute transport via advection/dispersion, and a reactive one considering solute transport, cation exchange, mineral dissolution/precipitation, and kinetic redox reactions. Heavy metals fate and transport was not implemented in this reactive model given the low concentrations in leachates found in both columns (Alessandrino et al., 2023) and (Alessandrino et al., 2022a) batch experiments and given that a full characterization of the reactivity of the solid phases was not available to constrain model results.

2.3. Solute transport

The movement and the fate of solutes in the subsurface is a complex phenomenon that is affected by various aspects, including flow nonuniformity and unsteadiness, physicochemical interactions between solutes and matrix, and the mechanism of solute spreading (Konikow, 2011). It has been demonstrated that modelling 1-D reactive transport using PHREEQC-3 is an effective way to simulate aqueous speciation, reaction paths, and reactive transport (Sprocati et al., 2019). For this study, dispersivity was set up for each cell to 0.02 m as reported by Alessandrino et al. (2022b), the diffusion coefficient was fixed to $2.59e^{-9}$ m^2/s, and the flow direction was set up as forward. The number of time steps in the advective-dispersive transport simulation was set up to 40 for the fertilizer injection (NPK or FW) followed by other 120 time steps for the flushing period with SRWP. Each time step was subdivided into 100 transport time steps of 1 s to minimize numerical oscillations. The initial pulse of fertilizer (NPK or FW) lasted for 4000 s (1.11 h) and was then flushed by SRWP for 12,000 s (3.33 h). The transport model used is the one defined by the Cauchy boundary condition (de Lange, 1999):

$$C(x,t) = C_0 + \frac{D_L}{v}\frac{\partial C(x,t)}{\partial x} \quad (1)$$

where C is the concentration of an *ith* species expressed in mmol/L in the position x and at the time t, C_0 is the initial concentration inside the column expressed in mmol/L, v is the flow velocity expressed in m/s, and D_L is the dispersion coefficient expressed in m^2/s.

Table 1
Chemical composition of the rainwater proxy (SRWP), NPK solution, and fertigation water (FW) used in the laboratory experiments.

	SRWP	NPK	FW
T	25 °C	25 °C	25 °C
pH	6.2	7.3	7.0
	mmol/L	*mmol/L*	*mmol/L*
DIC	0.8	–	–
Ca^{2+}	0.16	0.16	3.27
Mg^{2+}	0.005	0.01	1.02
Na^{+}	0.1	0.07	6.3
K^{+}	0.05	4.16	0.8
Cl^{-}	0.1	0.3	6.69
DOC	0.1	0.5	3.5
SOC	10	10	10
O_2	0.21	0.21	0.21
NH_4^+	0.04	0.15	0.81
PO_4^{3-}	0.001	1.41	0.04
NO_2^-	–	0.01	0.77
NO_3^-	–	2.29	0.03
SO_4^{2-}	–	0.01	0.66

2.4. Cation exchange

EXCHANGE data block was used to define the amount and composition of the exchanger and thus defining the CEC of soil and soil-graphene mixture. For all the experiments a generic exchanger *X-* was set up. For CS_NPK and CS_FW columns only one EXCHANGE 1–50 keyword was used for all the cells of the column. Two EXCHANGE keywords were used for the CSG_NPK, one for cells 1–10 and another one for cells 11–50 to discriminate the soil-graphene mixture (first 10 cm) from the remaining part of the column filled only with soil. For the same reason two EXCHANGE keywords were used for CSG_FW, one for cells 1–10 and another for cells 11–50.

2.5. Mineral dissolution/precipitation

The EQUILIBRIUM_PHASES data blocks were used to define the amounts of the main mineral phases that can react reversibly with the aqueous phase, here Calcite ($CaCO_3$), Dolomite ($CaMg(CO_3)_2$), and Hydroxyapatite ($Ca_5(PO_4)_3OH$). The saturation indexes for Calcite, Dolomite, and Hydroxyapatite were set to 0, while their initial moles were set to 10, $3e^{-4}$, and 0 mol, respectively. The initial moles estimates were done considering thin sections of sandy soil material analysed via optical microscope with polarized lenses.

2.6. Kinetic reactions

KINETICS data blocks were used to specify kinetic reactions and reactive-transport calculations of ammonium (NH_4^+), soil organic carbon (SOC), and dissolved organic carbon (DOC). For all the species and for all the columns the following parameters were used: 1 mol as current moles of reactant (m); 1 mol as initial moles of reactant (m_0), and $1e^{-8}$ mol as tolerance for integration procedure (tol). For the FW columns, the kinetic component of DOC adsorption (DOC_sorption) was added because of the high concentration of DOC in FW that can enhance organic carbon sorption by soil particles (Jardine et al., 1989). The parameters of this component were set to 0 mol as current moles of reactant and to $1e^{-8}$ mol as tolerance for integration procedure. RATES keyword was used to define the mathematical rate expressions for the kinetic reactions of NH_4^+, SOC, DOC, and DOC_sorption.

The following multiplicative Monod rate expression was used to describe the rate of nitrification:

$$R_{NH_4^+} = -q_{m(NH_4^+)}\frac{N_{NH_4^+}}{\left(K_{NH_4^+}+N_{NH_4^+}\right)}\frac{N_{O_2}}{(K_{O_2}+N_{O_2})} \quad (2)$$

where R_{NH4+} is the rate of nitrification expressed in mol/L/s, $q_{m(NH4+)}$ is the maximum nitrification rate constant, N_{NH4+} and N_{O2} indicate the moles of NH_4^+ and dissolved O_2 respectively, K_{NH4+} is the half saturation constant for NH_4^+, and K_{O2} is the half saturation constant for dissolved O_2.

The following Monod rate expression was used to describe the rate of DOC consumption via denitrification:

$$R_{DOC} = -q_{m(DOC)}\frac{N_{DOC}}{(K_{DOC}+N_{DOC})}\frac{N_{NO_3}}{\left(K_{NO_3}+N_{NO_3}\right)} \quad (3)$$

where R_{DOC} is the rate of DOC degradation expressed in mol/L/s, $q_{m(DOC)}$ is the maximum DOC degradation rate constant using NO_3^- as electrons acceptor, N_{DOC} and N_{NO3} indicate the molar concentration of DOC and NO_3^- respectively, K_{DOC} is the half saturation constant for DOC, K_{NO3} is the half saturation constant for NO_3^-.

The following Monod rate expression was used to describe the rate of the SOC degradation:

$$R_{SOC} = -q_{m(SOC)} \frac{N_{SOC}}{(K_{SOC} + N_{SOC})} \frac{N_{NO_3}}{(K_{NO_3} + N_{NO_3})} \quad (4)$$

where R_{SOC} is the rate of SOC degradation expressed in mol/L/s, $q_{m(SOC)}$ is the maximum SOC degradation rate constant using NO_3^- as electrons acceptor, N_{SOC} and N_{NO3} indicate the moles of DOC and NO_3^- respectively, K_{SOC} is the half saturation constant for SOC, K_{NO3} is the half saturation constant for NO_3^-.

DOC, as well as being a substrate for microorganisms' metabolism, has sorption affinities with soil aggregates (Kaiser et al., 2001), thus Tebes-Stevens et al. (1998) defined the kinetic reaction for DOC_sorption by the rate equation:

$$R_{DOC\_sorption} = -k_m \left(n_{DOC} - \frac{s_i}{K_d} \right) \quad (5)$$

where $R_{DOC\_sorption}$ is the rate of DOC_sorption expressed in mol/g/s, k_m is the mass transfer coefficient, K_d is the distribution coefficient, s_i is the sorbed species, and n_{DOC} indicates the moles of DOC.

2.7. Model performance evaluation

Model calibration was achieved via trial-and-error technique, manually tuning the initially guessed parameters until a satisfactory model performance was achieved. Three indices were used to examine the efficiency of the models: the Nash-Sutcliffe model efficiency coefficient (NSE), the R squared correlation index (R^2), and the index of agreement (d).

NSE measures how much the residual variance differs from the variance of the observed data (Nash and Sutcliffe, 1970) and it was obtained by the following equation:

$$NSE = 1 - \frac{\sum_{i=1}^{n} (OBS_i - SIM_i)^2}{\sum_{i=1}^{n} (OBS_i - \overline{OBS})^2} \quad (6)$$

where OBS_i is the observation value, SIM_i is the forecast value, and $\overline{OBS}$ is the average of the observation values. NSE = 1 corresponds to a perfect match between the observed and the modelled data; NSE = 0 indicates that the model's predictions are as accurate as the average of the observed data; NSE <0 indicates that the observed mean is a better predictor than the model.

R^2 is probably the most widely applied "goodness-of-fit" metric in modelling and prediction of environmental systems (Onyutha, 2021) and it was obtained by the following equation:

$$R^2 = 1 - \frac{SSR}{SST} \quad (7)$$

where SSR is the sum squared regression and SST is the total sum of squares. $R^2 = 1$ means that there is a perfect fit between the observed and the modelled data.

The index of agreement (d) is a standardized measure of the degree of model prediction error (Willmott, 1981). It was obtained using the following equation:

$$d = 1 - \frac{\sum_{i=1}^{n} (O_i - P_i)^2}{\sum_{i=1}^{n} (|P_i - \overline{O}| + |O_i - \overline{O}|)^2} \quad (8)$$

where O_i is the observation value, P_i is the forecast value, and $\overline{O}$ is the average of the observation values. d is the ratio of mean square error to potential error. A score of 1 shows a perfect match between the observed and modelled data, whereas a value of 0 indicates no agreement at all.

A sensitivity analysis was also performed on the calibrated model using perturbation tests of ±20 % and ± 50 % for the kinetic rates ($q_{m(NH4+)}$, $q_{m(DOC)}$, and $q_{m(SOC)}$) and for the X- values, to test whether small changes of the calibrated parameters may have an impact on the model performance indicators. The validation of the reactive model was achieved comparing the obtained model parameters versus literature values. Moreover, the multiple interactions of the modelled species, that cannot be calibrated singularly, allowed to narrow the possibility to find incorrect or implausible model parameters.

3. Results and discussion

3.1. NPK leaching modelling

Experimental and modelled data and the input of PHREEQC models are all reported in the Supplementary Information. The reactive model results matched the experimental data better than the non-reactive model for CS_NPK and CSG_NPK columns (Figs. 2 and 3). For instance, on negatively charged soil surfaces, cations such as Na^+, K^+, Mg^{2+}, Ca^{2+}, and NH_4^+ are generally adsorbed (Solly et al., 2020), thus CEC is one of the main processes regulating cation mobility in soil water interfaces (Saidi, 2012). Moreover, fertilization and soil improver application could influence, positively or negatively, the soil CEC (Pernes-Debuyser and Tessier, 2004). Indeed, it becomes apparent how implementing CEC within the modelling framework allowed for a dramatically better K^+ fitting respect to the non-reactive model. As for K^+, Na^+ fitting was also slightly improved after the inclusion of CEC in the reactive model. The employment of equilibrium mineral phases to simulate $CaCO_3$ and $CaMg(CO_3)_2$ precipitation and dissolution allowed a better match between Ca^{2+} observed data and modelled data in comparison to the non-reactive model. In fact, dissolution-precipitation is the main process occurring at mineral-water interfaces that control the biogeochemical cycle of several elements (Putnis, 2014). A mineral can dissolve in a fluid by reaching an equilibrium phase at the mineral-fluid interface; and conversely, a dissolved species can undergo supersaturation and thus precipitate (Wang and Putnis, 2020). This equilibration mechanism is critical for understanding a wide range of solid-fluid reactions as well as the possible application of innovative and functionally relevant materials such as graphene. It is clear how disregarding both CEC and equilibrium mineral phases, Ca^{2+} concentration was stable at 0.16 mmol/L for both CS_NPK and CSG_NPK columns. For the same reason, the non-reactive model did not show a good match between the observed and calculated data regarding Mg^{2+}, since the observed concentrations depend on the dissolution of $CaMg(CO_3)_2$ and CEC. Indeed, graphene incorporation increased by 40 % the CEC in the first 10 cm of the CSG_NPK column respect to the CS_NPK column. Two X- values were used in the graphene amended columns, one for the graphene/soil mixture and one for the soil. The calibrated X- value corresponding to the soil for NPK columns was very similar to the measured CEC (Alessandrino et al., 2022a). The difference in the calibrated X- values between the two layers highlighted the CEC increase due to graphene amendment because of its wide surface area and its strong positive functional groups (Geim and Novoselov, 2007; Wang et al., 2013). Splitting in two layers the X-values provided an excellent match with the observed cations, while the initial trials using a mean value for the whole column did not allow to reach good model performances (not shown). The observed increase in CEC through graphene application offers promising implications for sustainable soil management and nutrient retention. The greater retention of cations within the soil matrix can mitigate nutrient loss through leaching, thereby reducing the environmental impact associated with excessive fertilizer applications. Furthermore, the reduced mobility of cations can enhance their availability to plants, leading to improved nutrient uptake and potentially higher crop yields (Igwe and Nkemakosi, 2007). In addition, the assumption of equilibrium mineral phases for $Ca_5(PO_4)_3OH$ precipitation was necessary. In fact, very low PO_4^{3-} concentrations were simulated by the reactive model as those observed, while the non-reactive model showed an unrealistic breakthrough of PO_4^{3-} with a peak of up to

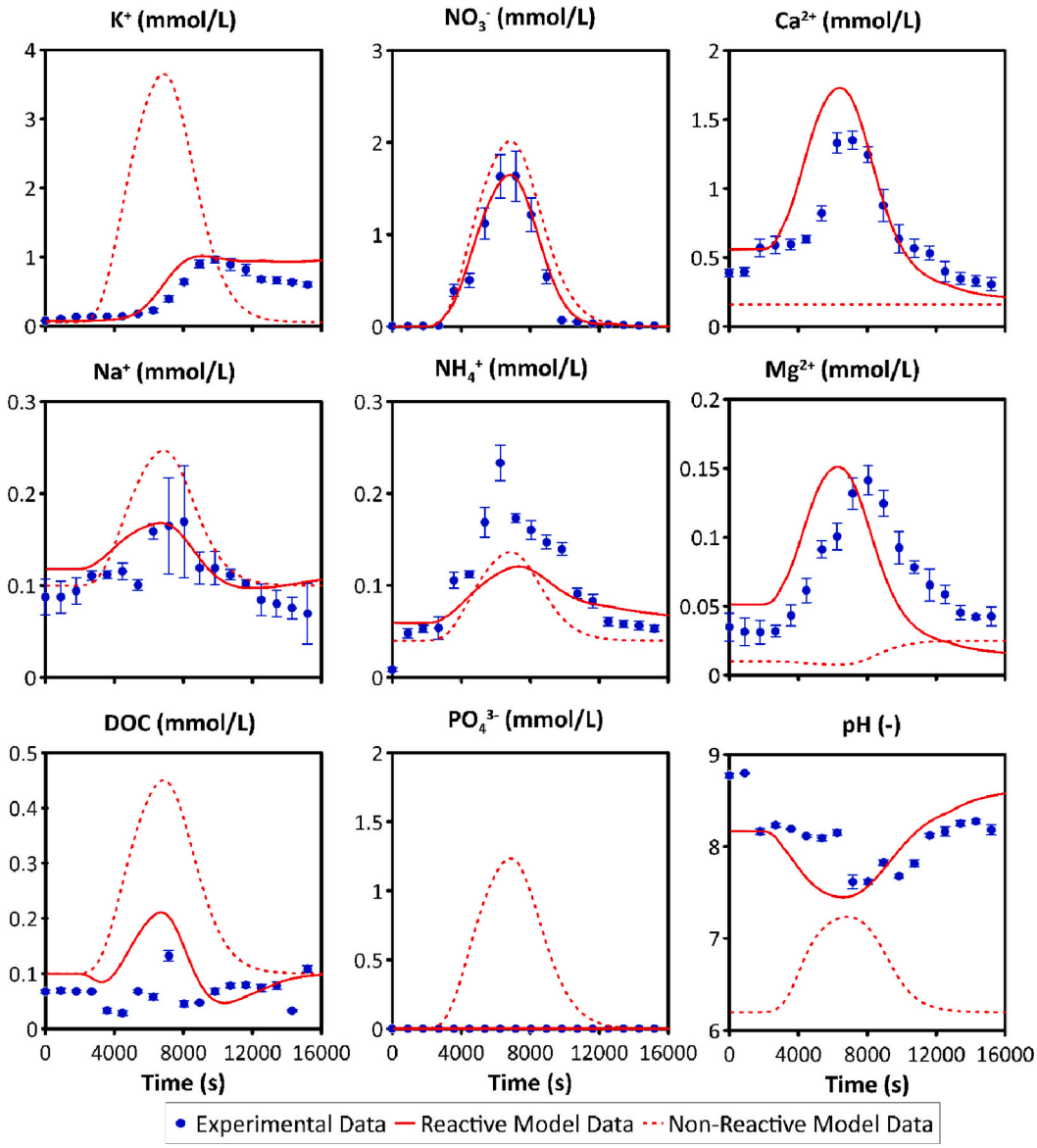

Fig. 2. Selected species and pH breakthrough curves of the CS_NPK column experiment. Observed data (blue dots) and their error bars (standard deviation on three replicas) versus the calibrated reactive model (red continuous line) and the non-reactive model (red dashed line).

1.2 mmol/L, given the high P amount in the NPK solution (Table 1). Further evidence that the assumed reactive network is robust is provided by the shifts in pH, well captured by the reactive models. The pH fluctuations, in fact, were most likely due to the precipitation of $Ca_5(PO_4)_3OH$, which was not included in the non-reactive model. Indeed, the precipitation of $Ca_5(PO_4)_3OH$ is governed by the following equation (Inskeep and Silvertooth, 1988):

$$Ca_5(PO_4)_3OH + 4H^+ \leftrightarrow H_2O + 3HPO_4^{-2} + 5Ca^{2+} \quad (9)$$

The consumption of H^+ ions for the precipitation of $Ca_5(PO_4)_3OH$ could have triggered the pH lowering during the experiment. Moreover, the presence of organics acids such as fulvic, humic, and citric acids in the porewater can inhibit $Ca_5(PO_4)_3OH$ precipitation (Inskeep and Silvertooth, 1988). Nevertheless, the NPK used in this study was free of organic acids (Table 1).

A good match among the observed DOC and the reactive model of the CS_NPK column was achieved tuning DOC and SOC kinetic parameters, while the non-reactive model showed an unrealistic DOC peak. A reasonable match among the observed and modelled DOC was also achieved in the CSG_NPK column, but the scattering of the observed DOC made the difference from the non-reactive model less evident than for CS_NPK column. It is known that the availability of electrons in organic carbon compounds is one of the most important factors controlling biological denitrification. In the absence of oxygen, biological denitrification happens naturally when certain bacteria employ nitrate as a terminal electron acceptor in their respiratory process consuming the DOC available in the porewater (Busico et al., 2021). Denitrification is a series of enzyme processes that result in the evolution of nitrogen gas. Several nitrogen intermediates are formed during the process, which can be simplified as follows (Soares, 200):

$$NO_3^- \xrightarrow[FeSMo]{\text{Nitrate reductase}} NO_2^- \xrightarrow[Cytochrome\ cd]{\text{Nitrite reductase}} NO \xrightarrow{\text{Nitric oxide reductase}} N_2O \times \xrightarrow{\text{Nitrous oxide reductase}} N_2 \quad (10)$$

Thus, considering the kinetic reaction of DOC consumption via heterotrophic denitrification, an excellent match among the observed and calculated NO_3^- concentrations was achieved in both CS_NPK and CSG_NPK reactive models. This has clearly demonstrated that heterotrophic denitrification was the driver that decreased NO_3^- leaching in the

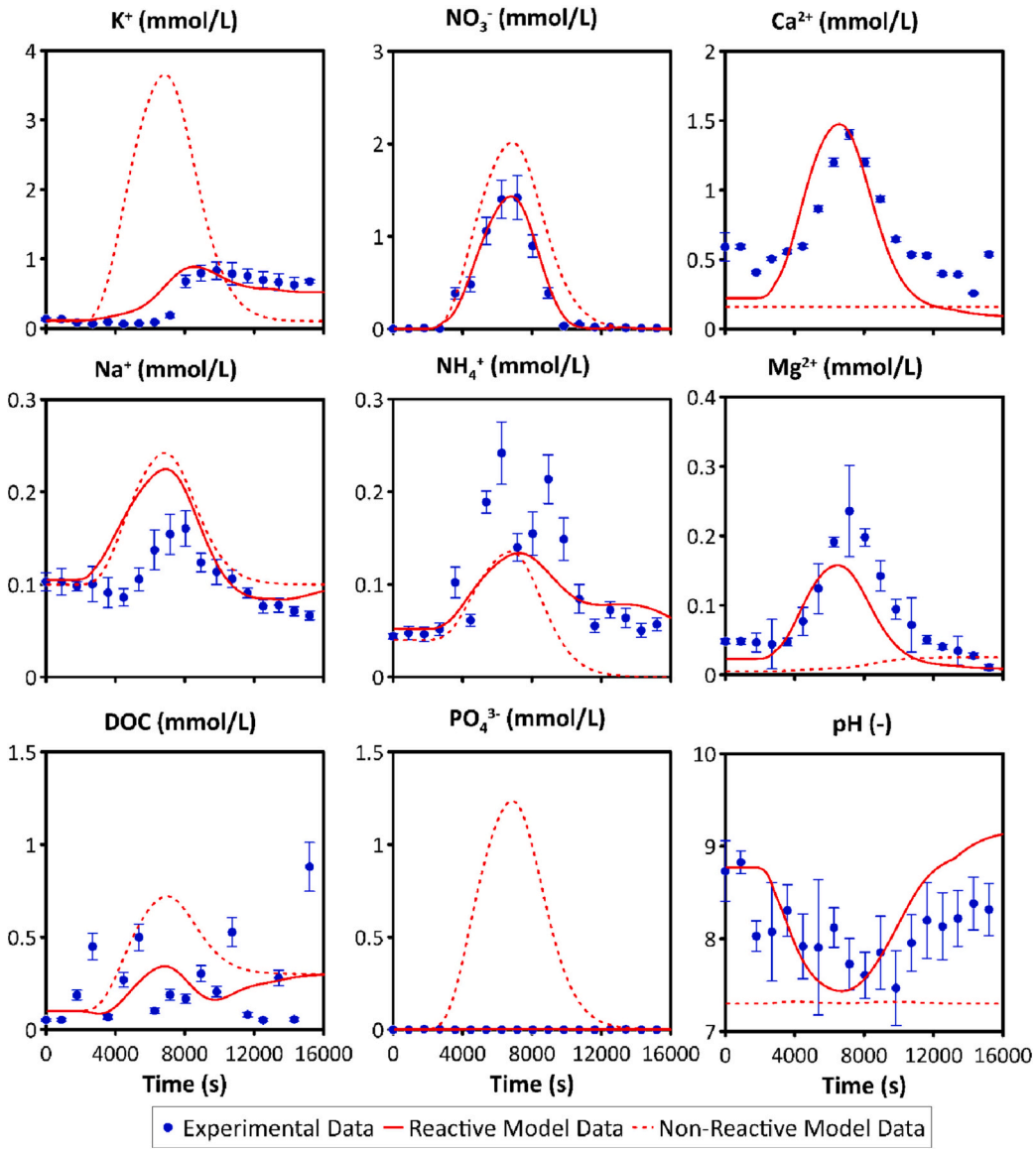

Fig. 3. Selected species and pH breakthrough curves of the CSG_NPK column experiment. Observed data (blue dots) and their error bars (standard deviation on three replicas) versus the calibrated reactive model (red continuous line) and the non-reactive model (red dashed line).

reactive models respect to the non-reactive ones. Graphene incorporation largely increased the $q_{m(DOC)}$ and $q_{m(SOC)}$ values (Table 2), using NO_3^- as the terminal electron acceptor. In fact, a study conducted by Ren et al. (2015) on the effect of graphene on soil bacterial community showed that graphene could enhance soil bacterial activity, thus augmenting organic carbon degradation. Additionally, Jiang et al. (2020) found that graphene enhanced bio-denitrification by promoting microorganisms' carbon sources metabolism. Previous reactive modelling studies in laboratory (Rodríguez-Escales et al., 2016) and field conditions (Lee et al., 2009) found much higher denitrification rates stimulated by adding carbon substrates, with values between $1.25e^{-3}$–$3.47e^{-4}$ mol/L/s for $q_{m(DOC)}$, and K_{NO3} values between $1.80e^{-4}$–$8.18e^{-6}$ mol/L. The differences among those rates and the ones here found are due to the carbon substrates used: easily degradable compounds like glucose, ethanol, fumarate were employed by Rodríguez-Escales et al. (2016) while in this study no labile carbon sources were added to feed the denitrifiers, which were then in limited carbon substrates availability, decreasing their denitrification capacity. Indeed, a recent review on field-based studies found a wide variety of denitrification rates (Li et al., 2022) with maximum values of $1.75e^{-8} \pm 16.2e^{-10}$ mol/L/s under humid subtropical climates usually rich in labile substrates, to minimum values of $3.99e^{-9} \pm 16.0e^{-10}$ mol/L/s in arid climates. The above-mentioned field denitrification rates for soils are one order of magnitude lower than the ones found in water saturated conditions and with labile substrates abundance. For example, Wang et al. (2020) found $q_{m(DOC)}$ values within a range of $1.8e^{-8}$–$4.5e^{-9}$ mol/

Table 2
Reactive parameters for each column experiment.

Parameter	CS_NPK	CSG_NPK	CS_FW	CSG_FW
X- 1-10 cm (mol/L)	$1.75e^{-02}$	$2.50e^{-02}$	$1.00e^{-02}$	$2.50e^{-02}$
X- 11-50 cm (mol/L)	$1.75e^{-02}$	$1.75e^{-02}$	$1.00e^{-02}$	$1.00e^{-02}$
$q^{+}_{m(NH4}$ (mol/L/s)	$3.30e^{-10}$	$3.30e^{-10}$	$8.80e^{-09}$	$1.00e^{-08}$
K_{NH4} (mol/L)	$1.10e^{-05}$	$1.10e^{-04}$	$1.10e^{-05}$	$1.10e^{-04}$
K_{O2} (mol/L)	$1.60e^{-05}$	$1.60e^{-05}$	$1.60e^{-05}$	$1.60e^{-05}$
$q_{m(DOC)}$, $q_{m(SOC)}$ (mol/L/s)	$7.70e^{-08}$	$1.10e^{-07}$	$8.80e^{-09}$	$1.00e^{-07}$
K_{DOC}, K_{SOC} (mol/L)	$1.10e^{-04}$	$1.00e^{-04}$	$1.00e^{-04}$	$1.00e^{-04}$
K_{NO3} (mol/L)	$1.00e^{-04}$	$1.00e^{-04}$	$1.00e^{-04}$	$1.10e^{-04}$
K_m (s^{-1})	–	–	$1.10e^{-04}$	$1.00e^{-03}$
S_i (mol g^{-1})	–	–	$3.75e^{+03}$	$3.75e^{+03}$
K_d (L g^{-1})	–	–	$2.00e^{-03}$	$2.00e^{-03}$

L/s in water saturated column's experiments and without labile substrates addition, are they also found increasing $q_{m(DOC)}$ with increasing NO_3^- concentrations. Those values are in agreement with the rates of the present study for the CS_NPK columns (Table 2). Moreover, graphene increased the $q_{m(DOC)}$ rate of >140 % in the columns treated with NPK. Heterotrophic denitrification was the only relevant terminal electron acceptor process in DOC and SOC degradation kinetics, given that the inclusion of oxygen did not improve the simulation results (not shown), since all the available oxygen was already consumed during nitrification. Other less favourable electron acceptors like Mn, Fe, and SO_4^{2-} were ruled out by thermodynamic constraints, since Eh never reached negative values, and by the low concentration of all the three redox sensitive species (Alessandrino et al., 2023). NH_4^+ modelling turns out to be complex because it was governed by CEC, nitrification, and could be released by bacterial decay (Barry et al., 2002). For the principle of model parsimony in reactive modelling (Schäfer Rodrigues Silva et al., 2020), bacterial growth and decay was assumed at steady state and consequently omitted.

3.2. FW leaching modelling

The reactive model matched the experimental data better than the non-reactive model also for CS_FW and CSG_FW columns, even if the differences were less pronounced than in the NPK column experiments (Fig. 4). As for NPK columns, the employment of equilibrium exchanger sites to model the soil CEC in the FW column experiments allowed to achieve a good fit among observed and calculated K^+ concentrations, producing a slight retardation respect to the non-reactive model. Indeed, graphene incorporation increased it by 150 % in the first 10 cm of the CSG_FW column in comparison with the CS_FW column.

Both the reactive and the non-reactive models show a good match with the observed Na^+ concentrations, given the relatively high concentrations of Na^+ in FW (Table 1). As stated for the NPK reactive models, also in the CS_FW and CSG_FW reactive models denitrification allowed a better match of DOC and NO_3^- concentrations respect to the non-reactive model. In the CS_FW and CSG_FW models, DOC sorption kinetics was also considered given the high DOC concentration in FW. To reach a good model calibration versus DOC, a one order of magnitude increase of k_m was necessary in the CSG_FW respect to the CS_FW column (Table 2), confirming that graphene has a good adsorption capacity of organic compounds (Wang et al., 2013). Lower values of $q_{m(DOC)}$ were found for CS-FW columns in this study in comparison with the ones found by Wang et al. (2020), likely due to the very low NO_3^- concentrations in the FW. Moreover, graphene incorporation involved one order of magnitude increase of the $q_{m(DOC)}$ rate. The difference between the NH_4^+ breakthrough curves obtained from the reactive and non-reactive models was due to $q_{m(NH4}^+$ and equilibrium CEC employed in the reactive model. Indeed, the maximum nitrification rate was $8.8e^{-9}$ mol/L/s for CS_FW and $1.0e^{-8}$ mol/L/s for CSG_FW (Table 2), nearly two orders of magnitude higher than the one found for the NPK columns. This was due to the high NH_4^+ concentrations in FW and to oxic conditions, which triggered the nitrification process as formerly pointed out in batch experiments with the same soil and FW (Alessandrino et al., 2022a). In fact, one of the main in-soil kinetic reaction is nitrification, that is the biological process by which ammonia (NH_3) or ammonium (NH_4^+) are converted by soil microorganisms to nitrite (NO_2^-) or nitrate (NO_3^-) according to the following reactions (Norton, 2008):

$$NH_3 + O_2 + 2H^+ + 2e^- \rightarrow NH_2OH + H_2O \rightarrow NO_2^- + 5H^+ + 4e^- \quad (11)$$

$$NO_2^- + H_2O \rightarrow NO_3^- + 2H^+ + 2e^- \quad (12)$$

In this study, no large differences among $q_{m(NH4}^+$ in graphene amended columns and controls were found (Table 2), suggesting that graphene is not capable to affect nitrification rates in water saturated conditions. Overall, the nitrification rates calculated for this study agree with the recent literature on nitrification in soils (Li et al., 2020). Due to the high NO_2^- input concentration in the FW, observed NO_2^- were compared versus calculated ones in the FW columns. NO_2^- was modelled as conservative species and in both CS_FW and CSG_FW columns modelled concentrations showed a good match with the observed ones. In all experiments the pH trend appeared to be very similar with an initial lowering followed by a rise. Since a plausible good model fit was achieved treating NO_2^- as a conservative species, this means that in similar systems NO_2^- can leached relatively undisturbed. This is a relevant information since NO_2^- leaching may be of concern in environments characterized by limited or refractory DOC (Mastrocicco et al., 2019) and could also trigger the emission of N_2O (Giguere et al., 2017) and nitrous acid from soils (Su et al., 2011). The reactive models captured the observed pH trend despite the large observed pH variability, in contrast to the non-reactive models that failed to reproduce such trend.

3.3. Model performance and sensitivity analysis

The quality control of the reactive models was granted using performance indicators and then via the sensitivity analysis varying the calibrated parameters as explained below. Fig. 5 shows that the calibrated model performance is satisfactory with an overall *d*, R^2, and NSE above 0.95, 0.80, and 0.78, respectively. The less performing one was the CSG_NPK model, due to a non-optimal fit on Na^+ and Mg^{2+}. Besides, Fig. 5 shows that changes in nitrification and denitrification rates did not dramatically affect the model performance indicators. In fact, R^2, *NSE*, and *d* values were slightly higher in the calibrated models than the perturbed ones, without large variations. It must be stressed that the results of the sensitivity analysis highlighted no substantial changes in all the model's performance indicators for perturbations of ±20 % of the nitrification and denitrification kinetic rates, while a more pronounced decrease was induced by a perturbation of ±50 % in the CSG_NPK column.

This finding underlines the robustness of the reactive parameters here found, characterized by a low degree of uncertainty. Finally, the sensitivity to the CEC *X*- values for both CS_NPK and CSG_NPK columns were higher than the sensitivity to nitrification and denitrification kinetic parameters, with an abrupt deterioration of all the model performance indicators for a −50 % decrease of *X*- values in the CS_NPK and CSG_NPK models. This clearly indicates the major role of CEC over nitrification and denitrification in the columns treated with NPK.

4. Conclusions

An integrated numerical model accounting for soil adsorption capacity and biogeochemical processes was developed to assess the main changes in the leaching behaviours triggered by graphene incorporation. The reactive model fitted the experimental data better than the nonreactive model, showing that the assumptions considered in the conceptual geochemical model are all essential. The main results of the study are summarized below:

- Combining experimental observations with a process-based transport model, this study demonstrated that graphene incorporation to the soil triggered an increase of denitrification rates. Indeed, $q_{m(DOC)}$ and $q_{m(SOC)}$ parameters showed a dramatic increase both in CSG_NPK and CSG_FW in comparison with the respective controls.
- Graphene incorporation increased soil CEC and DOC sorption capacity, demonstrating a good adsorption capacity for both inorganic cations and organic compounds, so decreasing nutrients leaching that represent a major concern related to agricultural practices. In fact, the X^- parameter was increased by 43 % in CSG_NPK and 150 % in CSG_FW in comparison with the respective controls. While the value of the K_m parameter was increased by an order of magnitude in CSG_FW compared to the control.

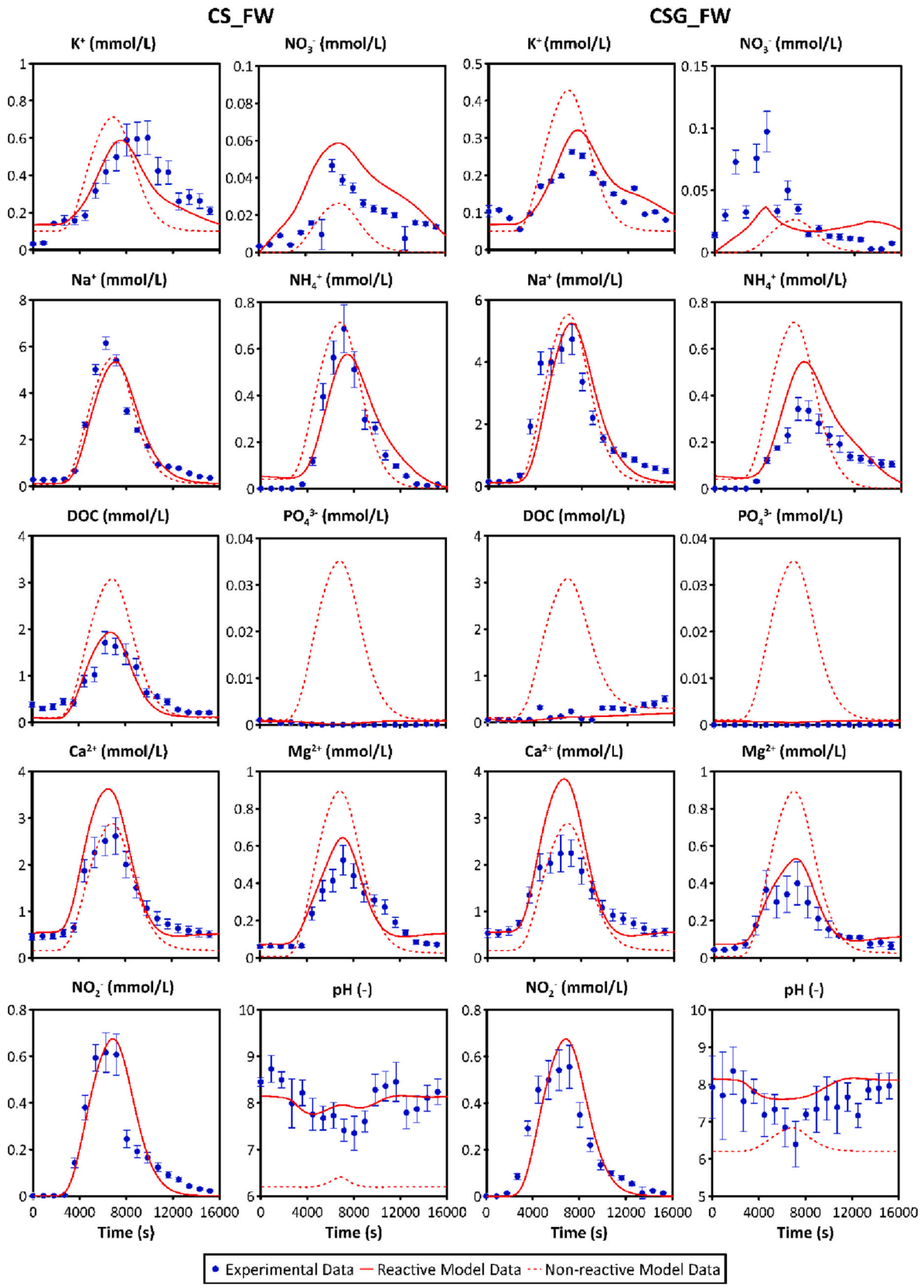

Fig. 4. Selected species and pH breakthrough curves of the CS_FW (left panels) and CSG_FW (right panels) column experiments. Observed data (blue dots) and their error bars (standard deviation on three replicas) versus the calibrated reactive model (red continuous line) and the non-reactive model (red dashed line).

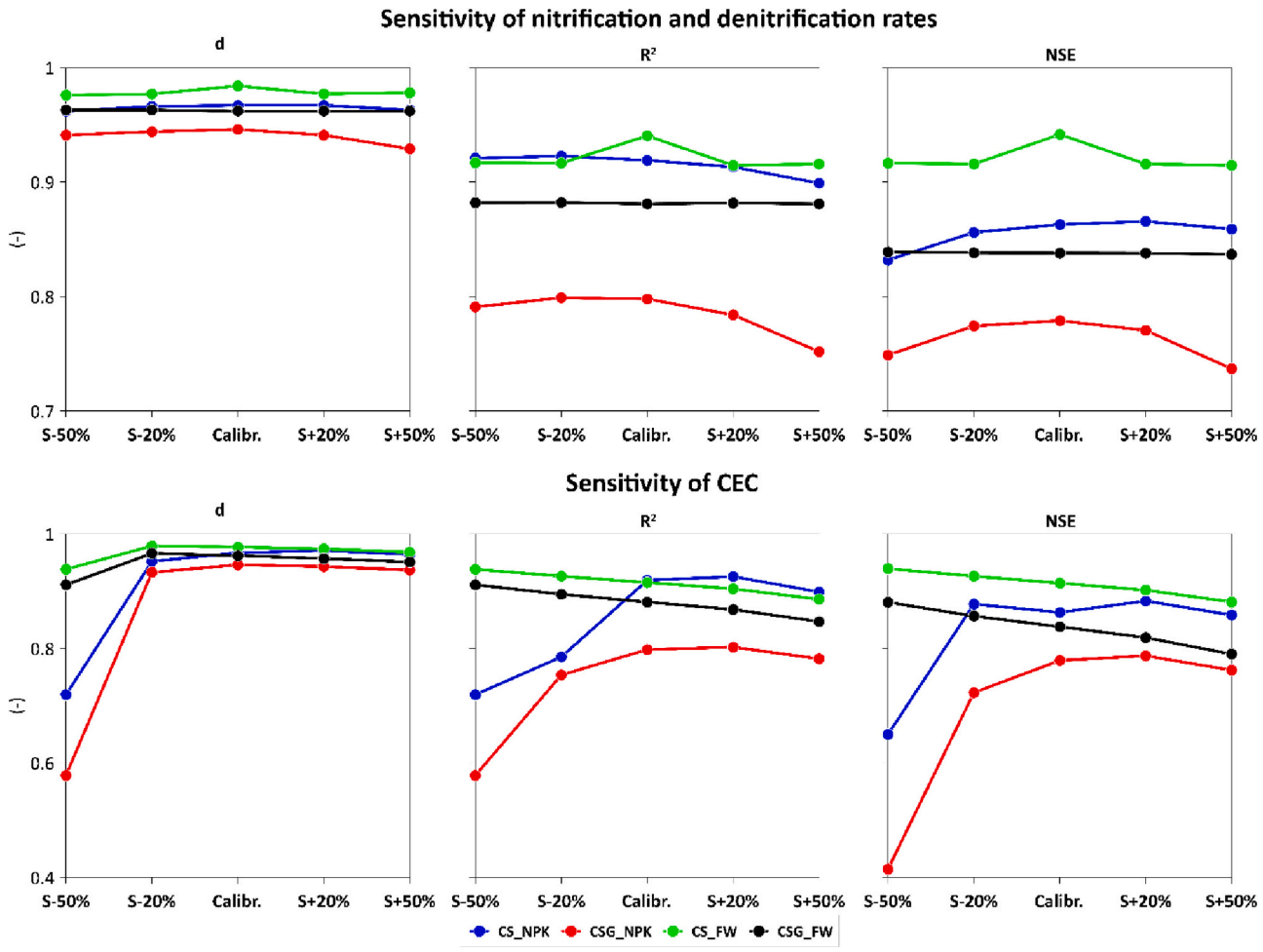

Fig. 5. Sensitivity analysis perturbing by ±20 % and ± 50 % the nitrification ($q^{+}_{m(NH4)}$) and denitrification ($q_{m(DOC)}$, $q_{m(SOC)}$) rates (upper panels), and the CEC (*X*-) exchange coefficient (lower panels).

- This model-based analysis of the column experiments suggested that the retention of PO_4^{3-} was due to $Ca_5(PO_4)_3OH$ precipitation and was not affected by graphene incorporation into the soil.
- The results obtained from the reactive models suggest that the use of innovative fertilizers that contain a high amount of DOC, such as FW from wastewater treatment plant, may result in a decrease of the soil CEC and may not limit NO_2^- leaching.

These results could be relevant for future graphene applications as a soil improver or as suitable material to enhance soil bioremediation in order to include graphene in a circular economy loop.

Despite the promising results obtained in in this study regarding the application of graphene to the soil, it is important to acknowledge that its widespread implementation still requires further investigation. Specifically, comprehensive studies focusing on the potential environmental spreading of graphene and its impact on plants and soil microbial communities are necessary. Understanding the fate and behaviour of graphene in the environment is crucial to ensure its safe and sustainable utilization in the long term. Research efforts should be directed towards assessing its potential interactions with various environmental compartments, including soil, water, and the biosphere.

CRediT authorship contribution statement

Luigi Alessandrino: Investigation, Software, Formal analysis, Data curation, Visualization, Writing – original draft. **Nicolò Colombani:** Conceptualization, Methodology, Software, Validation, Writing – review & editing, Visualization, Resources. **Micòl Mastrocicco:** Conceptualization, Validation, Writing – review & editing, Supervision.

Declaration of competing interest

The authors declare that they have no known competing financial interests or personal relationships that could have appeared to influence the work reported in this paper.

Data availability

Data will be made available on request.

Appendix A. Supplementary data

Supplementary data to this article can be found online at https://doi.org/10.1016/j.scitotenv.2023.165558.

References

Alessandrino, L., Colombani, N., Eusebi, A.L., Aschonitis, V., Mastrocicco, M., 2022a. Testing graphene versus classical soil improvers in a sandy calcisol. Catena. https://doi.org/10.1016/j.catena.2021.105754.

Alessandrino, L., Eusebi, A., Aschonitis, V., Mastrocicco, M., Colombani, N., 2022b. Variation of the hydraulic properties in sandy soils induced by the addition of graphene and classical soil improvers. J. Hydrol. 612, 128256 https://doi.org/10.1016/j.jhydrol.2022.128256.

Alessandrino, L., Colombani, N., Aschonitis, V., Eusebi, A.L., Mastrocicco, M., 2023. Performance of graphene and traditional soil improvers in limiting nutrients and

heavy metals leaching from a sandy Calcisol. Sci. Total Environ. 159806 https://doi.org/10.1016/j.scitotenv.2022.159806.
Bandala, E.R., Berli, M., 2018. Nanomaterials: new agrotechnology tools to improve soil quality? In: López-Valdez, F., Fernández-Luqueño, F. (Eds.), Agricultural Nanobiotechnology: Modern Agriculture for a Sustainable Future. Springer International Publishing, Cham, pp. 127–140. https://doi.org/10.1007/978-3-319-96719-6_7.
Barry, D.A., Prommer, H., Miller, C.T., Engesgaard, P., Brun, A., Zheng, C., 2002. Modelling the fate of oxidisable organic contaminants in groundwater. Adv. Water Resour. 25, 945–983. https://doi.org/10.1016/S0309-1708(02)00044-1.
Bethke, C.M., Brady, P.V., 2000. How the Kd approach undermines ground water cleanup. Groundwater 38, 435–443. https://doi.org/10.1111/j.1745-6584.2000.tb00230.x.
Busico, G., Alessandrino, L., Mastrocicco, M., 2021. Denitrification in intrinsic and specific groundwater vulnerability assessment: a review. Appl. Sci. 11 (22), 10657. https://doi.org/10.3390/app112210657.
Chan, K.Y., Van Zwieten, L., Meszaros, I., Downie, A., Joseph, S., 2007. Agronomic values of greenwaste biochar as a soil amendment. Aust. J. Soil Res. 45, 629–634. https://doi.org/10.1071/SR07109.
Dafny, E., Šimůnek, J., 2016. Infiltration in layered loessial deposits: revised numerical simulations and recharge assessment. J. Hydrol. 538, 339–354. https://doi.org/10.1016/j.jhydrol.2016.04.029.
de Lange, W.J., 1999. A Cauchy boundary condition for the lumped interaction between an arbitrary number of surface waters and a regional aquifer. J. Hydrol. 226, 250–261. https://doi.org/10.1016/S0022-1694(99)00143-2.
Di, H.J., Cameron, K.C., 2002. Nitrate leaching in temperate agroecosystems: sources, factors and mitigating strategies. Nutr. Cycl. Agroecosyst. 64, 237–256. https://doi.org/10.1023/A:1021471531188.
Ellmer, F., Peschke, H., Köhn, W., Chmielewski, F.-M., Baumecker, M., 2000. Tillage and fertilizing effects on sandy soils. Review and selected results of long-term experiments at Humboldt-University Berlin. J. Plant Nutr. Soil Sci. 163, 267–272. https://doi.org/10.1002/1522-2624(200006)163:3<267::AID-JPLN267>3.0.CO;2-Z.
Geim, A.K., Novoselov, K.S., 2007. The rise of graphene. Nat. Mater. 6, 183–191. https://doi.org/10.1038/nmat1849.
Giguere, A.T., Taylor, A.E., Suwa, Y., Myrold, D.D., Bottomley, P.J., 2017. Uncoupling of ammonia oxidation from nitrite oxidation: impact upon nitrous oxide production in non-cropped Oregon soils. Soil Biol. Biochem. 104, 30–38. https://doi.org/10.1016/j.soilbio.2016.10.011.
Gruba, P., Mulder, J., 2015. Tree species affect cation exchange capacity (CEC) and cation binding properties of organic matter in acid forest soils. Sci. Total Environ. 511, 655–662. https://doi.org/10.1016/j.scitotenv.2015.01.013.
Hardie, M., Clothier, B., Bound, S., Oliver, G., Close, D., 2014. Does biochar influence soil physical properties and soil water availability? Plant Soil 376, 347–361. https://doi.org/10.1007/s11104-013-1980-x.
Igwe, C.A., Nkemakosi, J.T., 2007. Nutrient element contents and cation exchange capacity in fine fractions of southeastern Nigerian soils in relation to their stability. Commun. Soil Sci. Plant Anal. 38 (9–10), 1221–1242. https://doi.org/10.1080/00103620701328347.
Inskeep, W.P., Silvertooth, J.C., 1988. Kinetics of hydroxyapatite precipitation at pH 7.4 to 8.4. Geochim. Cosmochim. Acta 52, 1883–1893. https://doi.org/10.1016/0016-7037(88)90012.
ISO 21268-3:2019 n.d. Soil quality — Leaching procedures for subsequent chemical and ecotoxicological testing of soil and soil-like materials — Part 3: Up-flow percolation test.
Jardine, P.M., McCarthy, J.F., Weber, N.L., 1989. Mechanisms of dissolved organic carbon adsorption on soil. Soil Sci. Soc. Am. J. 53 (5), 1378–1385. https://doi.org/10.2136/sssaj1989.03615995005300050013x.
Jiang, M., Feng, L., Zheng, X., Chen, Y., 2020. Bio-denitrification performance enhanced by graphene-facilitated iron acquisition. Water Res. 180, 115916 https://doi.org/10.1016/j.watres.2020.115916.
Kaiser, K., Kaupenjohann, M., Zech, W., 2001. Sorption of dissolved organic carbon in soils: effects of soil sample storage, soil-to-solution ratio, and temperature. Geoderma 99 (3–4), 0–328. https://doi.org/10.1016/s0016-7061(00)00077-x.
Konikow, L.F., 2011. The secret to successful solute-transport modeling. Groundwater 49 (2), 144–159. https://doi.org/10.1111/j.1745-6584.2010.00764.x.
Lee, E.J., Kim, M., Kim, Y., Lee, K.-K., 2009. Numerical and field investigation of enhanced in situ denitrification in a shallow-zone well-to-well recirculation system. Ecol. Model. 220, 2441–2449. https://doi.org/10.1016/j.ecolmodel.2009.06.014.
Li, Z., Zeng, Z., Tian, D., Wang, J., Fu, Z., Zhang, F., Zhang, R., Chen, W., Luo, Y., Niu, S., 2020. Global patterns and controlling factors of soil nitrification rate. Glob. Chang. Biol. 26, 4147–4157. https://doi.org/10.1111/gcb.15119.
Li, Z., Tang, Z., Song, Z., Chen, W., Tian, D., Tang, S., Wang, X., Wang, J., Liu, W., Wang, Y., Li, J., Jiang, L., Luo, Y., Niu, S., 2022. Variations and controlling factors of soil denitrification rate. Glob. Chang. Biol. 28, 2133–2145. https://doi.org/10.1111/gcb.16066.
Lin, L., Peng, H., Liu, Z., 2019. Synthesis challenges for graphene industry. Nat. Mater. 18 (6), 520–524. https://doi.org/10.1038/s41563-019-0341-4.
Mastrocicco, M., Colombani, N., Soana, E., Vincenzi, F., Castaldelli, G., 2019. Intense rainfalls trigger nitrite leaching in agricultural soils depleted in organic matter. Sci. Total Environ. 665, 80–90. https://doi.org/10.1016/j.scitotenv.2019.01.306.
Nash, J.E., Sutcliffe, J.V., 1970. River flow forecasting through conceptual models. Part I — a discussion of principles. J. Hydrol. 10, 282–290. https://doi.org/10.1016/0022-1694(70)90255-6.
Norton, J.M., 2008. Nitrification in agricultural soils. In: Schepers, J.S., Raun, W.R. (Eds.), Nitrogen in Agricultural Systems. https://doi.org/10.2134/agronmonogr49.c6.
Novak, J.M., Watts, D.W., 2004. Increasing the phosphorus sorption capacity of southeastern coastal plain soils using water treatment residuals. Soil Sci. 169 (3), 206–214. https://doi.org/10.1097/01.ss.0000122522.03492.30.
Novoselov, K.S., 2011. Graphene: materials in the flatland (Nobel lecture). Angew. Chem. Int. Ed. 50, 6986–7002. https://doi.org/10.1002/anie.201101502.
Onyutha, C., 2021. A hydrological model skill score and revised R-squared. Hydrol. Res. 53, 51–64. https://doi.org/10.2166/nh.2021.071.
Parkhurst, D.L., Appelo, C.A.J., 2013. Description of Input and Examples for PHREEQC Version 3: A Computer Program for Speciation, Batch-reaction, One-dimensional Transport, and Inverse Geochemical Calculations (No. 6-A43). USGS.
Paton, K.R., Varrla, E., Backes, C., Smith, R.J., Khan, U., Boland, C., Lotya, M., Istrate, O. M., King, P., Higgins, T., Barwich, S., May, P., Puczkarski, P., Ahmed, I., Moebius, M., Pettersson, H., Long, E., Coelho, J.E.S., O'Brien, S.E., McGuire, E.K., Sanchez, B.M., Duesberg, G.S., McEvoy, N., Pennycook, T.J., Dowing, C., Crossley, A., Nicolosi, V., Coleman, J.N., 2014. Scalable production of large quantities of defect-free few-layer graphene by shear exfoliation in liquids. Nat. Mater. 13 (6), 624–630. https://doi.org/10.1038/nmat3944.
Pernes-Debuyser, A., Tessier, D., 2004. Soil physical properties affected by long-term fertilization. Eur. J. Soil Sci. 55 (3), 505–512. https://doi.org/10.1111/j.1365-2389.2004.00614.x.
Plošek, L., Elbl, J., Lošák, T., Kužel, S., Kintl, A., Juřička, D., Kynický, J., Martensson, A., Brtnický, M., 2017. Leaching of mineral nitrogen in the soil influenced by addition of compost and N-mineral fertilizer. Acta Agric. Scand. B Soil Plant Sci. 67, 607–614. https://doi.org/10.1080/09064710.2017.1322632.
Putnis, A., 2014. Why mineral interfaces matter. Science 343, 1441–1442. https://doi.org/10.1126/science.1250884.
Reichert, J.M., Amado, T.J.C., Reinert, D.J., Rodrigues, M.F., Suzuki, L.E.A.S., 2016. Land use effects on subtropical, sandy soil under sandyzation/desertification processes. Agric. Ecosyst. Environ. 233, 370–380. https://doi.org/10.1016/j.agee.2016.09.039.
Reiss, T., Hjelt, K., Ferrari, A.C., 2019. Graphene is on track to deliver on its promises. Nat. Nanotechnol. 14 (10), 907–910. https://doi.org/10.1038/s41565-019-0557-0.
Ren, W., Ren, G., Teng, Y., Li, Z., Li, L., 2015. Time-dependent effect of graphene on the structure, abundance, and function of the soil bacterial community. J. Hazard. Mat. 297, 286–294. https://doi.org/10.1016/j.jhazmat.2015.05.017.
Rodríguez-Escales, P., Folch, A., van Breukelen, B.M., Vidal-Gavilan, G., Sanchez-Vila, X., 2016. Modeling long term enhanced in situ biodenitrification and induced heterogeneity in column experiments under different feeding strategies. J. Hydrol. 538, 127–137. https://doi.org/10.1016/j.jhydrol.2016.04.012.
Ruan, G., Sun, Z., Peng, Z., Tour, J.M., 2011. Growth of graphene from food, insects, and waste. ACS Nano 5, 7601–7607. https://doi.org/10.1021/nn202625c.
Saidi, D., 2012. Importance and role of cation exchange capacity on the physicals properties of the Cheliff saline soils (Algeria). Proc. Eng 33, 435–449. https://doi.org/10.1016/j.proeng.2012.01.1223.
Schäfer Rodrigues Silva, A., Guthke, A., Höge, M., Cirpka, O.A., Nowak, W., 2020. Strategies for simplifying reactive transport models: a Bayesian model comparison. Water Resour. Res. 56 (11), e2020WR028100 https://doi.org/10.1029/2020WR028100.
Şengör, S.S., Ünlü, K., 2023. Colloidal transport of heavy metals in low-advective-velocity environmental systems: reactive transport model on biogeochemical and hydrodynamic impacts. Vadose Zone J. 22 (1), e20233 https://doi.org/10.1002/vzj2.20233.
Solly, E.F., Weber, V., Zimmermann, S., Walthert, L., Hagedorn, F., Schmidt, M.W.I., 2020. A critical evaluation of the relationship between the effective cation exchange capacity and soil organic carbon content in Swiss forest soils. Front. For. Glob. Change 3, 98. https://doi.org/10.3389/ffgc.2020.00098.
Sprocati, R., Masi, M., Muniruzzaman, M., Rolle, M., 2019. Modeling electrokinetic transport and biogeochemical reactions in porous media: a multidimensional Nernst–Planck–Poisson approach with PHREEQC coupling. Adv. Water Resour. 127, 134–147. https://doi.org/10.1016/j.advwatres.2019.03.011.
Steefel, C.I., Mayer, K.U., Arora, B., Appelo, C.A.J., Hammond, G., Jacques, D., Kolditz, O., Lagneau, V., Lichtner, P.C., Meussen, H., Molins, S., Parkhurst, D.L., Shao, H., Simůnek, J., Van der Lee, J., Yabusaki, S.B., Yeh, G.T., 2015. Reactive transport codes for subsurface environmental simulation. Comput. Geosci. 19, 445–478. https://doi.org/10.1007/s10596-014-9443-x.
Su, H., Cheng, Y., Oswald, R., Behrendt, T., Trebs, I., Meixner, F.X., Andreae, M.O., Cheng, P., Zhang, Y., Pöschl, U., 2011. Soil nitrite as a source of atmospheric HONO and OH radicals. Science 1207687. https://doi.org/10.1126/science.1207687.
Sun, H., Zhou, S., Jiang, Y., Xi, X., Tan, Y., Zhang, G., Jiang, N., Zhou, T., Yin, X., Wang, M., Gao, B., 2022. Fate and transport of engineered nanoparticles in soils and groundwater. Emerg. Contam. Soil Groundw. Syst. 205–251 https://doi.org/10.1016/B978-0-12-824088-5.00003-3.
Tabish, T.A., Memon, F.A., Gomez, D.E., Horsell, D.W., Zhang, S., 2018. A facile synthesis of porous graphene for efficient water and wastewater treatment. Sci. Rep. 8, 1817. https://doi.org/10.1038/s41598-018-19978-8.
Tebes-Stevens, C., Valocchi, A.J., VanBriesen, J.M., Rittmann, B.E., 1998. Multicomponent transport with coupled geochemical and microbiological reactions: model description and example simulations. J. Hydrol. 209, 8–26. https://doi.org/10.1016/S0022-1694(98)00104-8.
Wang, L., Putnis, C.V., 2020. Dissolution and precipitation dynamics at environmental mineral interfaces imaged by in situ atomic force microscopy. Acc. Chem. Res. 53 (6), 1196–1205. https://doi.org/10.1021/acs.accounts.0c00128.

Wang, S., Sun, H., Ang, H.M., Tadé, M.O., 2013. Adsorptive remediation of environmental pollutants using novel graphene-based nanomaterials. Chem. Eng. J. 226, 336–347. https://doi.org/10.1016/j.cej.2013.04.070.
Wang, J., Ma, R., Guo, Z., Qu, L., Yin, M., Zheng, C., 2020. Experiment and multicomponent model based analysis on the effect of flow rate and nitrate concentration on denitrification in low-permeability media. J. Contam. Hydrol. 235, 103727 https://doi.org/10.1016/j.jconhyd.2020.103727.
White, P.J., Crawford, J.W., Díaz Álvarez, M.C., García Moreno, R., 2014. Soil management for sustainable agriculture 2013. Appl. Environ. Soil Sci. 2014, 536825 https://doi.org/10.1155/2014/536825.
Willmott, C.J., 1981. On the validation of models. Phys. Geogr. 2, 184–194. https://doi.org/10.1080/02723646.1981.10642213.
Zhang, Y., Hu, B., Teng, Y., Tu, K., Zhu, C., 2019. A library of BASIC scripts of reaction rates for geochemical modeling using phreeqc. Comput. Geosci. 133, 104316 https://doi.org/10.1016/j.cageo.2019.104316.
Zurutuza, A., Marinelli, C., 2014. Challenges and opportunities in graphene commercialization. Nat. Nanotechnol. 9 (10), 730–734. https://doi.org/10.1038/nnano.2014.225.

Glossary

C: concentration
C_0: initial concentration
CEC: cation exchange capacity
CS_FW: calcareous sandy soil under a fertilization regime with fertigation water
CS_NPK: calcareous sandy soil under a NPK fertilization regime
CSG_FW: calcareous sandy soil amended with graphene under a fertilization regime with fertigation water
CSG_NPK: calcareous sandy soil amended with graphene under a NPK fertilization regime
d: index of agreement
DIC: Dissolved inorganic Carbon
D_L: dispersion coefficient
DOC: dissolved organic carbon
Eh: oxidation potential
FW: Fertigation Water
HDPE: high density polyethylene
K_d: distribution coefficient
K_{DOC}: half saturation constant for DOC
k_m: mass transfer coefficient
K_{NH4+}: half saturation constant for NH_4^+
K_{NO3}: half saturation constant for NO_3^-
K_{O2}: half saturation constant for dissolved O_2
K_{SOC}: half saturation constant for SOC
N: molar ratio
n: number of moles
NSE: Nash-Sutcliffe model efficiency coefficient
OBS_i: observation value (NSE calculation)
O_i: observation value (d calculation)
P_i: forecast value (d calculation)
$q_{m(DOC)}$: maximum DOC degradation rate constant
$q_{m(NH4+)}$: maximum nitrification rate constant
$q_{m(SOC)}$: maximum SOC degradation rate constant
R^2: R squared correlation index
R_{DOC}: rate of DOC degradation
$R_{DOC\_sorption}$: rate of DOC_sorption
R_{NH4+}: nitrification rate
R_{SOC}: rate of SOC degradation
s_i: sorbed species
SIM_i: forecast value (NSE calculation)
SOC: soil organic carbon
SRWP: synthetic rainwater proxy
SSR: sum squared regression
SST: total sum of squares
t: time
v: flow velocity